Progress in Oceanography
February 2015, Volume 131, Pages 33-45
http://dx.doi.org/10.1016/j.pocean.2014.11.008
http://archimer.ifremer.fr/doc/00238/34908/

Mediterranean outflow transports and entrainment estimates from observations and high-resolution modelling

Barbosa Aguiar Ana [1, 4, 6, *], Peliz Alvaro [1], Neves F. [2], Bashmachnikov I. [2, 3], Carton Xavier [4, 5]

[1] Instituto Dom Luiz, Faculdade de Ciências, Universidade de Lisboa, Campo Grande, 1749-016 Lisboa, Portugal
[2] Centro de Oceanografia, Faculdade de Ciências, Universidade de Lisboa, Campo Grande, 1749-016 Lisboa, Portugal
[3] Departamento de Engenharia Geográfica, Geofísica e Energia (DEGGE), Faculdade de Ciências, Universidade de Lisboa, Campo Grande, 1749-016 Lisboa, Portugal
[4] Laboratoire de Physique des Océans, UMR6523 CNRS/IFREMER/UBO, UFR Sciences, Brest, France
[5] UBO, France
[6] CNRS, France

* Corresponding author : Ana Barbosa Aguiar, email address : aaaguiar@fc.ul.pt

Abstract :

We use cross-slope sections of direct current observations together with a high resolution numerical simulation to revisit estimates of transports and entrainment in the Gulf of Cadiz. We provide a three dimensional picture of the outflow from the Mediterranean into the intermediate layers of the Atlantic. In the model, the time-averaged Mediterranean Undercurrent is characterised by two cores of zonal velocity at 8°30′8°30′W: one at 500 m (in the σ1σ1 interval 31.6-31.831.6-31.8 kg m-3) and another around 1100 m (~32.2~32.2 kg m-3) with maximum westward velocity of 0.36 m s-1. A single well defined vein of saltier and warmer water (salinity maximum ~36.9~36.9 psu, 1 psu = 1 kg salt/1000 kg seawater) is found attached to the slope, centred at 1300 m (32.2-32.432.2-32.4 kg m-3). The observational sections corroborate this description but instant maximum velocity reaches 0.6 m s-1 whereas salinity peaks just above 36.5 psu. Unlike what was previously thought, the velocity veins and the thermohaline anomaly cores are not co-located. At the Strait of Gibraltar, we estimate that the transport of pure Mediterranean Water (S>38.4S>38.4 psu) is about 0.48 Sv (1 Sv=106=106 m3s-1). Near the Portimão Canyon, the results for westward transport (31.6-32.631.6-32.6 kg m-3) computed from observations are within the range 2.6-3.62.6-3.6 Sv and the time-mean estimate from the numerical simulation is of 3.5 Sv. The westward salinity and heat transports are of ≲1.3≲1.3 psu Sv (1 psu Sv =103=103 m3s-1) and ~20×1012~20×1012 W, from observational and numerical data alike. By tracking water masses within a closed domain in the Gulf of Cadiz, we find that most of the North Atlantic Water entrained into the undercurrent is supplied through the south and southwest borders. After analysing volume balances per layer, we conclude that the entrainment from shallower layers is around 1.1 Sv in total: 0.32, 0.34, 0.40 and 0.04 Sv distributed by four equally spaced density intervals (0.2 kg m-3) between isopycnals 31.8 and 32.6 kg m-3.

Highlights

► MU velocity veins and thermohaline anomaly cores are not co-located ► Westward volume transport in observations is 2.6–3.6 Sv and in model is 3.5 Sv ► Westward salinity and heat transports are of ~1.3 psu Sv and ~20 × 10^{12} W ► Total entrainment of 1.1 Sv NACW from Lagrangian analysis in closed domain in GoC ► Most of the NACW entrained comes from the south and southwest borders

Keywords : Mediterranean outflow, Gulf of Cadiz, Volume transport, Entrainment, Diapycnal mixing, Lagrangian analysis

1. Introduction

The horizontal density gradient between the Mediterranean Sea and the North Atlantic Water forces a two-layer exchange flow at the Strait of Gibraltar: North Atlantic Water inflowing eastwards on surface levels and Mediterranean Water (MW) outflowing westwards as a bottom layer. The Mediterranean outflow veers northwards due to the Coriolis effect and progresses along the continental slope in the northern Gulf of Cadiz (GoC) as a density current: the Mediterranean Undercurrent (MU) (e.g., Ambar and Howe, 1979a, Ambar and Howe, 1979b and Ochoa and Bray, 1991).

Downstream from the Strait of Gibraltar, the outflow splits in two main veins characterised by two maxima in temperature and salinity profiles: the upper core MU_uMUu (σ_1=31.9)σ1=31.9) kg m^{-3}) centred at about 800 m, and the lower core MU_lMUl (σ_1=32.25)σ1=32.25) kg m^{-3}) centred at about 1200 m Ambar and Howe, 1979a and Ambar et al., 2002. Along its path, the outflow undergoes transformation by mixing with overlying North Atlantic Central Water (NACW) and underlying North Atlantic Deep Water (NADW). It reaches neutral buoyancy near 8°8°W (Bower et al., 2002).

There have been several attempts to estimate the volume transport associated to the MW outflow (e.g., Zenk, 1975, Ochoa and Bray, 1991 and Baschek et al., 2001). The reported estimates of westward transport of MW in the Strait of Gibraltar range from 0.9 to 1.8 Sv, but the more recent ones point to 0.77 Sv (García-Lafuente et al., 2011). Baringer and Price, 1997 suggest that 0.4 Sv (of their total 0.7 Sv) is pure Mediterranean Water, i.e. water with salinity $S \geq 38.4$ psu. Estimates of westward transport of transformed MW in the western GoC range from 2.9 to 3.7 Sv (e.g., Zenk (1975); Rhein and Hinrichsen (1993)), pointing to a five-fold increase of the initial volume. However, most of these values are somewhat uncertain because they are obtained by indirect methods such as models that require *a priori* assumptions.

Despite the importance of the entrainment toward the salinity distribution at intermediate layers in the North Atlantic, estimates of its magnitude are rare (Baringer and Price, 1997; Alves et al., 2011) and the entrainment of Atlantic Water into these levels remains poorly understood. Existent datasets are very limited in time and their geographical distribution is not suitable for defining a closed domain where to compute volume balances and diapycnal mixing.

Here we use a large set of hydrology observations and direct cross-slope velocity measurements to reassess the paths and properties of the outflow along the GoC slope. These observations are used for validation and in combination with our numerical data, output from a high-resolution numerical simulation taylor-made to realistically reproduce the Mediterranean-Atlantic exchanges over 10 years. Furthermore, we run a Lagrangian analysis over the numerical data (particle seeding experiments) to track different water masses inside a closed domain. Such analysis provided a unique insight into the 3D evolution of the MW outflow and the general circulation within the GoC, allowing for direct estimates of diapycnal entrainment.

Both observational and numerical datasets are described in the next section, while the methods and data analysis applied are explained in section 3. The analysis and interpretation of the data for shelf sections is provided in section 4.1, while the quantitative Lagrangian analysis of the numerical data is detailed in section 4.2. Finally, the main results are highlighted and discussed in the closing section 5.

2. Data

2.1. Observations

Hydrographic and velocity measurements were collected during four campaigns in the GoC, off the Portuguese south coast: three cuises of the project Semane, in July 1999 (Semane1999), July 2000 (Semane2000.1) and September 2000 (Semane2000.2), and a cruise conducted in the framework of the project Sflux, in September 2011 (Figure 1, Table 1). Table 1 summarises some relevant information regarding the acquisition of the observational data. All the cruises occurred in the months of July and September during summer conditions. The sections are perpendicular to the bathymetry contours, covering the GoC northern slope from 7°25′W to 8°44′W. The length of the sections from the Sflux campaign ranges from around 20 to 50 km, whereas the majority of the Semane sections were originally longer than 70 km.

2.1.1. Semane

During the Semane cruises, horizontal current velocity was measured by a RDI 150 kHz broadband LADCP (Lowered Acoustic Doppler Current Profiler). For the Semane1999 cruise, the LADCP was configured with 22 bins of 8 m for bottom depths lower than 2000 m and 12 bins of 16 m for bottom depths larger than 2000 m. For cruises Semane2000.1 and Semane2000.2, the LADCP was configured with 22 bins of 8 m for bottom depths lower than 1000 m and 12 bins of 16 m for bottom depths below 1000 m. The LADCP data were processed with the SHOM-CMO (French Navy Hydrographic and Oceanographic Service) processing sequence. Measurements corresponding to large tilts of the ADCP, or with strong deviations in vertical velocities, were discarded and a median filter was applied. The velocities' error was about 2.5 cm s^{-1}.

The hydrographic data were collected with a SeaBird SBE911 CTD (Conductivity Temperature Depth) probe. Sections from the Semane cruises were essentially meridional and originally extended from the Portuguese to the Moroccan slope (except the Semane2000.2).

Both the hydrographic and current velocity data were interpolated, using the nearest neighbour method, to fill in the existing gaps. A low-pass Butterworth filter (of order 1 and cut-off wave number of 0.008 m^{-1}) was applied to reduce small-scale noise in the vertical direction. Finally, the data was interpolated onto a grid with a horizontal and vertical resolution of 500×5 m^2, respectively.

While some of these data were already used for computing volume transports in previous studies (e.g., Alves et al. (2011)), here we will analyse the transport in finer density layers obtaining the first (to our knowledge) detailed description of the vertical structure of the MW outflow. In addition, advective salinity and heat transports will be computed. Only the data collected north of 36°N is further studied herein.

2.1.2. Sflux

The data from the Sflux campaign were obtained aboard the RV Mytilus during days 16-23 of September 2011. The survey covered part of the continental slope in the southern Iberian peninsula. The data on the upper ocean were collected with a vessel-mounted RDI Workhorse 300 kHz broadband ADCP, configured with a bin size of 2 m and the ensemble interval of 1 minute. The ship navigated at a speed of 3-4 knots to achieve maximum accuracy in the ADCP survey. The initial processing of ADCP data was done using Cascade-Exploitation software provided at `http://wwz.ifremer.fr/lpo/Produits/Logiciels` To avoid the effect of "bubble noise" the segments of the trajectory where the ship's speed exceeded 5 knots were discarded (Atkinson, 2008). The segments of the trajectory during which the ship's speed dropped below 1 knot (CTD stations) were also discarded. This was done to reduce errors induced by abrupt changes in ship heading (King and Cooper, 1993).

The bin at 21-27 m depth was taken for the reference-level, as a trade-off between the best bin quality and the maximum distance from the sea-surface. Then the standard procedure of "Cascade-Exploitation" was used to flag bad or doubtful data (Le Bot et al., 2011) and only the data of the best quality were further used. The lowest limit of good data varied from 60 to 90 m. The current measurements of best quality were interpolated onto a regular grid with a vertical spacing of 10 m and a time interval of 4 minutes.

Finally, the velocity component orthogonal to the ship's trajectory was computed to merge with CTD derived geostrophic currents.

ADCP corrected geostrophic current

The CTD data were obtained with SeaBird SBE9 CTD, along seven sections (five cross-slope and two along-slope) with 1-2 miles stations' spacing. Using Defant's method the optimum zero-depth was defined as the minimum of the vertical gradient of dynamic depth at 250 m (Sheng and Thompson, 1996). Then the geostrophic currents were computed and corrected with upper ocean ADCP measurements. For this purpose, the ADCP currents were interpolated to the positions of the CTD stations and averaged over the layer 40-60 m. This layer was chosen as the part of the ADCP current profiles containing reliable data below the Ekman layer depth. The Ekman layer depth was computed (Bowden, 1983) using wind speed measured by the ship's anemometer to be on average 23 m, never exceeding 40 m depth. Analysis of the ADCP data showed that the most energetic small-scale oscillations in the upper layer were internal waves with periods of 1 and 2 hours, especially pronounced near the coast. To avoid the variable bias, a 3-hour moving average was applied to the layer-mean ADCP currents.

The difference between the 40-60 m mean ADCP and CTD currents was around 8 cm s^{-1}. The CTD-based geostrophic current profiles were corrected for the differences obtained.

2.2. Modelling output

A complete description of the configuration and model-data comparison is presented in Peliz et al. (2013). Here, we provide a short overview of the most important characteristics of the model.

The simulations were based on the Regional Ocean Modeling System version described in Shchepetkin and McWilliams (2005) forced with a 9 km resolution atmospheric forcing from a ERA-Interim regional downscaling solution using the Weather Research and Forecast system (Soares et al., 2012). The model grid resolution is uniform and around 2 km. In the vertical, 32 terrain-following levels are used with moderate stretching ($\theta_s = 4, \theta_b = 0$) in order to provide a good resolution in depth.

A key feature of the model is an adequate representation of the Atlantic-Mediterranean exchanges at the Strait. The exchanges (inflow and outflow) respond to the density difference between basins and to local winds and their difference is equal to the barotropic mass balance. The internal density structure is initialised and then nudged on the boundaries to climatological values.

In the western side of the Strait, strong lateral shear coupled with a sharp tracer gradient leads to an overshoot that was avoided by locally enhancing mixing and diffusion. This was achieved by using a Smagorinsky mixing coefficient in a region of 30 km in radius (centred at 35°54′N, 6°09′W) and depths below 200 m (see Peliz et al. (2013)).

A total of 20 years (1989-2008) were simulated and the output data corresponds to 2 day averages. In order to facilitate the data processing, here we will only analyse the output between 1989 and 1998. This is a representative period since previous studies (Baringer and Price, 1997; Peliz et al., 2013) indicate that no major inter-decadal changes should be expected in this region, in spite of non-negligible changes in hydrological properties in the MW outflow over the past 20-30 years (Millot et al., 2006).

The present study covers only the Atlantic side of the original simulation's domain, as represented in Figure 2.

3. Methods

3.1. Transports across shelf sections

Transports were calculated for potential density referenced to 1000 m (σ_1) to favour a more accurate description at larger depths.

Special attention was given to the density range corresponding to the spread of MW on the northern slope of the GoC: $31.6 - 32.6$ kg m^{-3} in σ_1. Such limits were set after analysing the model's output along a meridional section at 8°30′W and north of 36°24′N (see Figure 3, section II). Within this range, the volume, salinity and heat transports were computed for every 0.2 kg m^{-3} density layer. See Appendix A for details of the calculation.

This study focuses in transports by the MU and to ensure that only MW of the slope current was taken into account, the data was filtered by applying a "MW mask" (see section 4.2.1, Table 3) combined with a maximum offshore distance of 55 km (see Figure 4). Applying such mask will prevent taking into account water that did not mix with Mediterranean Water.

3.2. Tracking Mediterranean and Atlantic Water in the Gulf of Cadiz

These experiments were executed with the offline mass-conserving Lagrangian ARIANE scheme (Blanke and Raynaud (1997); Blanke et al. (1999); `http://www.univ-brest.fr/lpo/ariane`). This numerical tool represents the water masses by defining numerous small water parcels (particles) in user-specified locations. Using the three-dimensional velocity fields of ROMS's experiment, ARIANE time-integrates the trajectories of the synthetic particles until these cross the boundaries of a pre-defined closed domain.

As proposed by Blanke et al. (1999), each particle is allocated an individual weight related to the local magnitude of the Eulerian transport over the seeding section. The best initial positioning is achieved by grouping particles in regions where the transport is the highest, so that their individual weight is comparable and never exceeds a prescribed threshold (1×10^4 m^3 s^{-1} = 0.01 Sv). Particles initialized within the same model grid cell are allotted the same weight, but this weight is variable across neighboring grid cells.

Each particle conserves its volume along its trajectory and thus the transport across a section will be given by the sum of the individual volumes of all particles crossing that section, normalised by the number of times of seeding. Although not shown here, we checked that the estimates of total Lagrangian transport across each section (computed with ARIANE) were similar to those of Eulerian transport computed as described in Appendix A.

Our domain of study is delimited by the four geographical sections sketched in Figure 2. The seeding of particles can be performed along any section and be restricted to a chosen range of density, salinity and/or temperature. The temperature and salinity of the particles are allowed to evolve in time and space according to the local Eulerian fields provided by ROMS.

4. Results

4.1. Transports across shelf sections

4.1.1. Observations

In Figure 4 are given the salinity and zonal velocity fields of three sections from Semane2000.2, while the respective volume transports at intermediate layers ($31.6 < \sigma_1 \leq 32.6$ kg m^{-3}) are shown in Figure 5. These fields were chosen for the purpose of illustration because they cover three distinct meridional sections and correspond to data from the same campaign. In all these sections the Mediterranean undercurrent can be easily identified albeit with differences in intensity.

The strongest and deepest westward velocity reached values of ~ 0.6 m s^{-1}, recorded in the easternmost section (S06). Two well defined cores of different spatial extension but comparable intensity can be observed in the velocity fields: one just below 500 m and a larger one centred at about 1000-1200 m (see Figure 4). In S05 and S04 the MU is weaker (than in S06), especially the upper core which holds values of ~ 0.2 m s^{-1}.

In the salinity field, a single vein can be seen attached to the slope and with maximum salinity above 36.5 psu. The patch of more saline water extends farther off-shore than the intense westward velocities. In S04, at the southern edge of the vein, there is a blob of saline water which is likely to be a Meddy in formation, as corroborated by the anticyclonic zonal velocity signal: eastward (westward) on the northern (southern) edge of the blob. Note that, to restrict the computation of transports to the MU, the latter feature is filtered out after discarding all data beyond 55 km from the coast.

In sections S06 and S05, the total westward transport is 3.47 Sv and 3.23 Sv. The total westward salinity and heat transports (Figure 5) are about 1.2 psu Sv and 20×10^{12} W, respectively. Per density layer, these transports can be in excess of 0.4 psu Sv and 8×10^{12} W.

In section S04, the westward transport, salinity and heat transports in the MW layers are approximately 2 Sv, 0.6 psu Sv and 9×10^{12} W, respectively, about half as much as in S05 and S06.

For the sake of completeness, the westward transports for all the observational sections are listed in Table 2. The Sflux observations (S07-S10) contain only information from the upper core of the MU, since the lower one was not surveyed in this campaign.

4.1.2. Model: $\lambda \sim 8°30' W$, south from the coast to $\phi \geq 36°24' N$

The time-averaged model results are shown in Figure 6 for the short meridional shelf section at the longitude of Portimão Canyon, denoted as section II in the Lagrangian experiments below (see Figure 2). The fields of zonal velocity, salinity and temperature are displayed along with the volume, salinity and heat transports per density interval.

The time-averaged MU exhibits two distinct cores of zonal velocity at this location: one centred at 500 m ($31.6 - 31.8$ kg m^{-3}) and another one at 1100 m ($\sim 32.1 - 32.3$ kg m^{-3}), with maximum westward velocity about 0.36 m s^{-1}. However, only a single well defined vein of saltier and warmer water can be seen with a salinity (temperature) maximum $\sim$ 36.9 psu (12°C) attached to the slope around 1300 m ($32.2 - 32.4$ kg m^{-3}).

The bars in black (thick lines) overlayed in the graph of volume transport in Figure 6 indicate the amount of volume that originates in the Strait of Gibraltar. The difference between grey and black bars is due to entrainment/mixing of MW with fresher and colder Atlantic Water. The ongoing mixing is evident in Figure 3 where the TS-curves for section II "elbow" at temperatures and salinities ($\sim$ 12°C, 35.7 psu) well below those of the TS-curves for a section near Espartel ($\sim$ 14°C, 36 psu). The source and rates of mixing will be determined in section 4.2.2.

The total westward salinity and heat transports are about 1.3 psu Sv and 19×10^{12} W, respectively. In layer $32.2 - 32.4$ kg m^{-3}, these transports reach peak values of $\sim$ 0.5 psu Sv and $\sim 8 \times 10^{12}$ W that double those in any other layer.

4.1.3. Mediterranean Water transports: model versus observations

The results from the model and all Semane sections are summarised in Figure 7. We recall that a mask (Table 3) was applied when computing the volume transports, to exclude any flow other than that within the MU.

The volume transport of MW reached a maximum of 3.60 Sv in section S02, closely followed by 3.47 Sv in section S06, two geographically coincident sections just upstream of Portimão Canyon (see Figure 1). The lowest transport of 1.85 Sv was recorded at section S04, the only section downstream of Portimão Canyon. Sections S02, S03 and S06 are geographically coincident but refer to different time periods (Table 1) which may explain why the transport in S03 (2.61 Sv) is lower than in the other two. Section S01 overlaps with S05 but is shorter than the latter and thus its smaller volume transport is not surprising. At the exception of S04, in all sections from Semane the volume transport was most intense in the $32-32.2$ kg m^{-3} layer which contains most of the lower core as seen in Figure 4.

The model's shelf section exhibits an average transport of 3.51 Sv that is close to the 3.23 Sv computed from observational data at the same location (S05). Note that the model's transport is largest in layer $32.2-32.4$ kg m^{-3}, one layer below that with the peak transport in observations. Also, the numerical data show significant transport in layer $32.4-32.6$ kg m^{-3} whereas all the observations exhibit null values there.

Regarding the salinity and heat transports, layer $32.2-32.4$ kg m^{-3} holds the largest transports: ~ 0.6 psu Sv and $\sim 11 \times 10^{12}$ W, both recorded in section S02. The same happens in the model where the values for that layer are also twice as much as in any other layer. Overall, the salinity and heat transports in the model are consistent with those of the observations, in summary: $\lesssim 1.3$ psu Sv and $\sim 20 \times 10^{12}$ W.

4.2. Tracking Mediterranean and Atlantic Water in the Gulf of Cadiz

4.2.1. Pure Mediterranean Water

The main goal of this first Lagrangian experiment was to identify the pure MW flowing from the Strait of Gibraltar to the northern shelf of the GoC. Here, pure MW was defined as the water mass with $S > 38.4$ psu at section I (5°30′W), based on previous studies (Baringer and Price, 1997; Millot, 2009).

Particles were released sequentially every two days at section I, and integrated forward in time until crossing one of the other sections or reaching 2 months of age. More than 99% of the particles exit the domain within that time.

In Figure 8 are represented the time-averaged zonal-velocity, salinity and temperature fields at section I (5°30′W) along with the corresponding volume transport. The bars' graph represents the volume transport across the whole water column, showing that the inflow and outflow are in equilibrium at this location. The TS-diagram for section I is given in Figure 3.

At 5°30′W, the Lagrangian transport of pure MW is of 0.48 Sv (see Figure 2). About 98% of the particles heading west reach section II and thus the total transport recorded there (0.47 Sv) is approximately the same as in the seeding section.

All these particles leave section I concentrated in layer $\sigma_1 > 32.6$ (Figure 8) but as the pure MW enters the GoC it is transformed by mixing with Atlantic Water and the particles spread out to lower density layers.

In Figure 9 are given the percentage of particles and volume transport distributed by density layer upon arrival to section II. The vast majority of particles (70%, 0.33 Sv) ends up in layer $32.2 - 32.4$ kg m^{-3} while 11.6% and 11.2% spread to the immediately adjacent layers. This suggests that most of the pure MW flows in the lower core MU_l (centred at 32.25 kg m^{-3}) while only a very small portion ($< 8\%$) goes in the upper core MU_u (centred at 31.9 kg m^{-3}).

Based on the properties of particles (of original pure MW) that cross section II (8°30′W) we defined a mask for MW. The particles' mean salinity and temperature values plus or minus three standard deviations were taken as the extreme values corresponding to MW in each of the 0.2 kg m^{-3} thick density layers between 31.6 and 32.6 kg m^{-3}. These limits are listed in Table 3 and were applied to model's and observations' shelf sections data alike, restricting the computation of volume transport in section 4.1 to the flow of the MU.

4.2.2. Transports and entrainment estimates in a closed domain

In order to determine the pathways and volume transport of the water masses flowing through the closed domain shown in Figure 2, each of the four sections was seeded in turns in four independent Lagrangian experiments. Particles were released every two days in the whole water column and integrated forward in time until they either exit the closed domain or reach 4 months of age (or 2 months, when seeding section I). In most of the cases, more than 95% of the particles exit the domain but in the upper levels this value could drop to 90% in some periods.

The time-averaged fields of sections II and IV are displayed altogether in Figure 10, whereas those of section III are shown in Figure 11.

The overall results of the four experiments are sketched in Figure 12. The section of origin is represented in black and the arrows are in the colour of the respective section of arrival which is colorcoded as in Figure 2. Each arrow is tagged with the total volume transport of the flow it represents. In this figure are represented the volume exchanges in the whole water column – the total volume is conserved.

Nearly all flow entering the domain through section I (MW) reaches section II at a rate of 0.7 Sv, with only 0.01 Sv arriving at IV while 0.06 Sv return to the Mediterranean Sea.

From section II (NACW), 0.4 Sv recirculate and exit back through II while 0.2 Sv enter the Mediterranean Sea.

Section III (NACW) delivers 2 Sv to II, 1.2 Sv to IV and 0.4 Sv to I, with about 1 Sv being returned back southwards.

Finally, section IV (NACW) appears as the main Atlantic Water gateway to the closed domain, supplying 4 Sv that recirculate back to IV, 2 Sv to III, 1.8 Sv to II and 0.1 Sv to I.

Table 4 lists the total transports out (positive) and into (negative) the domain, per section and density layer. All the values displayed are rounded to 2 decimal places. However, the totals were computed using the full precision available which explains some discrepancies between these and the sum of the values given.

Since the volume is conserved in the domain, the balance per density layer gives a direct estimate of the overall diapycnal mixing (see Table 4, column 'Balance'). As expected, both shallow and deep layers lose mass into the intermediate layers: 1.09 Sv from overlying lighter waters and 0.77 Sv from denser waters of MW source. All the volume that enters the domain in the deepest layer (section I) is forced to exit through shallower layers (see column 'Total_I'). The amount of entrainment of NACW is then the remainder of 'Balance'-'Total_I' which is illustrated in Figure 13. Layers $31.8-32$, $32-32.2$, $32.2-32.4$ and $32.4-32.6$ kg m^{-3} entrain 0.32 Sv, 0.34 Sv and 0.40 Sv, 0.04 Sv of NACW.

To check if there was any entrainment of NADW, we recomputed the density of the particles as σ_2 (using $z = 2000$ m as reference depth), selected those with $\sigma_2 \geq 36.9$ kg m^{-3} and computed the associated Lagrangian transports across sections II, III and IV. The results are given in the last line of Table 4: only 0.09 Sv are entrained from NADW into intermediate layers.

Figure 14 illustrates the volume exchanges within three main layers: shallow ($\sigma_1 < 31.6$ kg m^{-3}, mostly NACW), intermediate ($31.6 \leq \sigma_1 < 32.6$ kg m^{-3}, MW mixed with NACW and NADW) and deep ($\sigma_2 \geq 36.9$ kg m^{-3}, mostly NADW).

In the intermediate layer, 2.15 Sv of NACW arrive to section II: 0.26 Sv through II itself, 0.83 Sv from III and 1.06 Sv from IV. Since the amount of MW exiting the domain through sections I, III and IV is negligible, we can assume that the total diapycnal mixing (Figure 13) refers to flow through II. This sets an upper limit of 3.25 Sv (2.15 Sv same-layer plus 1.1 Sv cross-layer) for the total volume of NACW that mixes with the outflow exiting through II.

It should be stressed that the transports indicated in Figure 12 and the sum of the values in the three main layers of Figure 14 are not comparable. First, there is a discontinuity in the density reference depth used in the latter: the mismatch is larger in section IV due to the larger fraction of seeding in the area below 2000 m. Second, unlike Figure 12, the results in Figure 14 do not include diapycnal mixing from/to layers above and below.

5. Concluding remarks

Near 8°30′W, in observational and numerical data, the Mediterranean Undercurrent exhibits two distinct cores of zonal velocity. One inshore at 500 m ($31.6 - 31.8$ kg m^{-3}) and another offshore at 1100 m (~ 32.2 kg m^{-3}), with maximum time-averaged westward velocity around 0.36 m s^{-1} (model) and peak values of 0.6 m s^{-1} (observations). A single well defined vein of saltier and warmer water is found (salinity maximum of 36.9 psu–model or 36.5 psu–observations), attached to the slope around 1300 m ($32.2 - 32.4$ kg m^{-3}). This confirms that the structure of the undercurrent consists of two main veins. However, the upper velocity core found herein appears at shallower depths than its thermohaline counterpart commonly reported to be centred around 750 m (e.g., Ambar and Howe (1979a); Baringer and Price (1997)). In summary, unlike what was previously thought, velocity veins and thermohaline anomaly cores are not co-located and this result is robust across the observed and modelled sections studied here.

Regarding the transport by the Mediterranean Undercurrent (westward flow within the density interval $31.6 - 32.6$ kg m^{-3} and using a mask), the results from the observations convey a total rate of $3.2 - 3.6$ Sv which is in very good agreement with the 3.5 Sv obtained from the model's output. Furthermore, these values are very close to those in Rhein and Hinrichsen (1993) where a total transport of 3.4 Sv was estimated at a meridional section near 8°30′W, assuming a transport of 1 Sv at the Strait and defining the Mediterranean outflow as $S > 36.2$ psu.

Near the Portimão Canyon, our estimates of salinity and heat transports from both observations and model are similar: $\lesssim 1.3$ psu Sv and $\sim 20 \times 10^{12}$ W for the respective total westward transports at intermediate layers. In the observations, the volume transport is most intense in layer $32.0 - 32.2$ kg m^{-1}, whereas the salinity and heat transports are often most intense in the layer $32.2 - 32.4$ kg m^{-1} below. The largest salinity and heat transports recorded in an individual layer are of ~ 0.6 psu Sv and $\sim 11 \times 10^{12}$ W.

After *in situ* measurements in the Strait, Bryden et al. (1994) estimated that the westward salinity transport was of 1.50 psu Sv. Although this refers to a location different than ours, both results are consistent since ours are computed further west and thus slightly smaller transports are expected as the outflow becomes more diluted. We did not find in the literature any observation-based estimates of heat transport in this region.

At 5°30′W (Figure 8), we have that the time-averaged westward (eastward) transport amounts to 0.78 Sv (0.84 Sv), based in numerical modelling. This is in agreement with the results of 0.76 Sv (0.81 Sv) by Baschek et al. (2001). It is also consistent with the result of García-Lafuente et al. (2011) and just slightly larger than earlier estimates of 0.7 Sv by Bryden et al. (1994) or Baringer and Price (1997).

Within the outflow, we estimate that the volume of pure Mediterranean Water (defined as $S > 38.4$ psu) is of 0.48 Sv, which is very close to the value of 0.4 Sv inferred by Baringer and Price (1997) for the same salinity criteria and using hydrographic data across the Strait. Almost all of this volume follows the continental shelf, reaching the Portimão Canyon (section II) within the density interval $32 - 32.4$ kg m^{-3} that comprises the Mediterranean Undercurrent's lower core. Conversely, the Mediterranean Undercurrent upper core at $31.8 - 32$ kg m^{-3} includes very little pure Mediterranean Water while receiving a relatively large amount of entrained water from shallower levels.

The westward transport of Mediterranean Water estimated at the shelf sections is seven times larger that of pure Mediterranean Water, suggesting that about 3 Sv of Atlantic Water are entrained in the process of water mass transformation of the outflow as it progresses along the northern boundary of the Gulf of Cadiz.

Computing the net volume transports per density layer in a closed domain, we were able to estimate the amount of ongoing diapycnal mixing as fresher water from the shallow layer (NACW) is entrained into intermediate layers. The layers $31.8-32$, $32-32.2$ and $32.2-32.4$ kg m^{-3} entrain 0.32, 0.34 and 0.40 Sv, respectively, while the denser layer $32.4 - 32.6$ kg m^{-3}, absorbs only 0.04 Sv. The overall time-averaged diapycnal mixing of NACW into the intermediate layers is about 1.1 Sv which is one order of magnitude larger than the diapycnal mixing of NADW (0.09 Sv). This result is not incompatible with the higher estimates of $1.21 - 1.67$ Sv by Alves et al. (2011) (see their Figure 10) since the latter depend on the constraints chosen for the inverse model used therein. In addition, the dominant transport from sections III and IV to section II confirms the cyclonic circulation in the Gulf of Cadiz also described in that study. In particular, the main influx from section IV might be linked to the usual cyclonic recirculation path followed by Meddies forming in the Portimão Canyon (Carton et al., 2002; Barbosa Aguiar et al., 2013). Our result for diapycnal mixing is also supported by a recent study by Carracedo et al. (2014) where the authors estimate a value of 1.2 Sv for the total volume of NACW that is transformed in the Gulf of Cadiz, based in another inverse model.

Within intermediate layers, the mean westward transport through section II corresponds approximately to the sum of: (i) same-layers mixing of NACW $\sim$ 2.15 Sv $= 0.26 + 0.83 + 1.06$ Sv from II, IV and III respectively; (ii) diapycnal mixing of NACW $\sim$ 1.1 Sv; and (iii) transport arriving from the Strait $\sim$ 0.72 Sv. Here, the mixing component (i) is deliberately not called lateral or isopycnal because it corresponds to transports within $31.6 - 32.6$ kg m^{-3} (Figure 14), where the density of the particles may vary but not enough to cross the isopycnal limits set. From this perspective, the total westward transport through section II amounts roughly to 4 Sv which compares well with the 3.5 Sv obtained from Eulerian transports, taking into account that the latter was computed by filtering out water that did not mix with the Mediterranean Water.

In general, the model results are close enough to the existing observations to lend credibility to the new results obtained herein, some of which could not be produced without resorting to numerical simulations.

Acknowledgments

This study had the support of Fundação para a Ciência e Tecnologia (FCT) through the projects MedEx (MARIN-ERA/MAR/0002/2008) and Sflux (PTDC/MAR/100677/2008). A.C.B.A. was funded by FCT through the Grant SFRH/BPD/64099/2009. I.B. acknowledges the contract C2008-UL-CO-3 between FCT and the University of Lisbon and the Center of Oceanography of the University of Lisbon. We wish to thank SHOM for the Semane data, the crew of RV Mytilus for their support during the Sflux campaign and Bruno Blanke for his invaluable guidance on ARIANE. We are also grateful for the comments and suggestions of the anonymous reviewers that helped to substantially improve the original manuscript.

References

Alves, J.M.R., Carton, X., Ambar, I., 2011. Hydrological structure, circulation and water mass transport in the Gulf of Cadiz. International Journal of Geosciences 2, 432–456.

Ambar, I., Howe, M.R., 1979a. Observations of the Mediterranean outflow - I Mixing in the Mediterranean outflow. Deep-Sea Research 26, 535–554.

Ambar, I., Howe, M.R., 1979b. Observations of the Mediterranean outflow - II The deep circulation in the vicinity of the Gulf of Cadiz. Deep-Sea Research 26, 555–568.

Ambar, I., Serra, N., Brogueira, M.J., Cabeçadas, G., Abrantes, F., Freitas, P., Gonçalves, C., Gonzalez, N., 2002. Physical, chemical and sedimentological aspects of the Mediterranean outflow off Iberia. Deep-Sea Research II 49, 4163–4177.

Antonov, J., Locarnini, R., Boyer, T., Mishonov, A., Garcia, H., 2006. World Ocean Atlas 2005 Volume 2: Salinity. NOAA Atlas NESDIS 62, U.S. Government Printing Office, Washington, D.C.

Atkinson, C., 2008. Analysis of shipboard ADCP data from RRS Discovery Cruise D324: RAPID Array Eastern Boundary. Technical report 12. National Oceanography Centre Southampton. Southampton, UK.

Barbosa Aguiar, A., Peliz, A., Carton, X., 2013. A census of meddies in a long-term high-resolution simulation. Progress in Oceanography 116, 80 – 94.

Baringer, M.O., Price, J.F., 1997. Mixing and Spreading of the Mediterranean Outflow. J. Physical Oceanogr. 27, 1654–1677.

Baschek, B., Send, U., Lafuente, J.G., Candela, J., 2001. Transport estimates in the strait of Gibraltar with a tidal inverse model. J. Geophys. Res. 106, 31033–31044.

Blanke, B., Arhan, M., Madec, G., Roche, S., 1999. Warm water paths in the equatorial atlantic as diagnosed with a general circulation model. J. Physical Oceanogr. 29, 2753–2768.

Blanke, B., Raynaud, S., 1997. Kinematics of the Pacific Equatorial Undercurrent: An Eulerian and Lagrangian Approach from GCM Results. J. Physical Oceanogr. 27, 1038–1053.

Bowden, K.F., 1983. Physical Oceanography of Coastal Waters. Ellis Horwood Ltd.

Bower, A., Serra, N., Ambar, I., 2002. Structure of the Mediterranean undercurrent and Mediterranean water spreading around the southwestern Iberian Peninsula. J. Geophys. Res. 107, C10,3161.

Bryden, H.L., Candela, J.C., Kinder, T.H., 1994. Exchange through the Strait of Gibraltar. Progress in Oceanography 33, 201–248.

Carracedo, L., Gilcoto, M., Mercier, H., Pérez, F., 2014. Seasonal dynamics in the AzoresGibraltar Strait region: A climatologically-based study. Progress in Oceanography 122, 116 – 130.

Carton, X., Chérubin, L., Paillet, J., Morel, Y., Serpette, A., Le Cann, B., 2002. Meddy coupling with a deep cyclone in the Gulf of Cadiz. J. Marine Sys. 32, 13–42.

Chambers, D., Tapley, B., Stewart, R., 1997. Long-period ocean heat storage rates and basin-scale heat fluxes from TOPEX. J. Geophys. Res. 102, C5, 10525–10533.

García-Lafuente, J., Sánchez-Román, J., Naranjo, C., Sánchez-Garrido, J.C., 2011. The very first transformation of the Mediterranean outflow in the Strait of Gibraltar. J. Geophys. Res. 116, C07010.

King, B., Cooper, E., 1993. Comparison of ships heading determined from an array of GPS antennas with heading from conventional gyrocompass measurements. Deep-Sea Research 40, 2207–2216.

Le Bot, P., Kermabon, C., Lherminier, P., Gaillard, F., 2011. CASCADE V6.1: Logiciel de validation et de visualisation des mesures ADCP de coque. Rapport technique OPS/LPO 11-01. Ifremer, Centre de Brest. France.

Locarnini, R., Mishonov, A., Antonov, J., Boyer, T., Garcia, H., 2006. World Ocean Atlas 2005 Volume 1: Temperature. NOAA Atlas NESDIS 61, U.S. Government Printing Office, Washington, D.C.

Millot, C., 2009. Another description of the Mediterranean Sea outflow. Progress in Oceanography 82, 101 – 124.

Millot, C., Candela, J., Fuda, J.L., Tber, Y., 2006. Large warming and salinification of the Mediterranean outflow due to changes in its composition. Deep Sea Research Part I: Oceanographic Research Papers 53, 656 – 666.

Ochoa, J., Bray, N.A., 1991. Water mass exchange in the Gulf of Cadiz. Deep-Sea Research 38, 465–503.

Peliz, A., Boutov, D., Cardoso, R., Delgado, J., Soares, P., 2013. The Gulf of Cadiz-Alboran Sea sub-basin: Model setup, exchange and seasonal variability. Ocean Modelling 61, 49–67.

Rhein, M., Hinrichsen, H., 1993. Modification of Mediterranean Water in the Gulf of Cadiz, studied with hydrographic, nutrient and chlorofluoromethane data. Deep Sea Research Part I: Oceanographic Research Papers 40, 267 – 291.

Shchepetkin, A.F., McWilliams, J.C., 2005. The regional oceanic modeling system (ROMS): a split-explicit, free-surface, topography-following-coordinate oceanic model. Ocean Modelling 9, 347–404.

Sheng, J., Thompson, K.R., 1996. A robust method for diagnosing regional shelf circulation from scattered density profiles. J. Geophys. Res. 101, 25647–25659.

Soares, P., Cardoso, R., de Medeiros, J., Miranda, P., Belo-Pereira, M., Espirito-Santo, F., 2012. WRF high resolution dynamical downscaling of ERA-interim for Portugal. Clim. Dyn. 39, 2497–2522.

Warren, B., 1999. Approximating the energy transport across oceanic sections. J. Geophys. Res. 104, C4, 7915–7919.

Zenk, W., 1975. On the Mediterranean outflow west of Gibraltar. "Meteor" Forsch.-Ergebnisse A, 23–34.

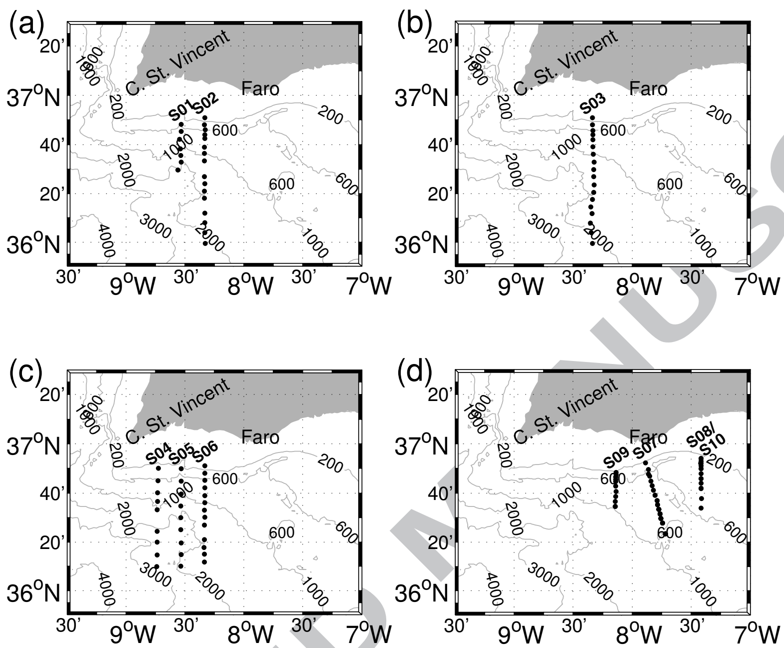

Figure 1: Maps of the Gulf of Cadiz showing the locations of the sections occupied during the campaigns (a) Semane1999, (b) Semane2000.1, (c) Semane2000.2 and (d) Sflux.

Table 1: Summary of the information on the observational data used in this paper.

Campaign	Date	Section	Longitude	Length (km)	Instruments
Semane1999	07/1999	S01	08°32′W	34.6	LADCP+CTD
		S02	08°20′W	95.2	
Semane2000 .1	07/2000	S03	08°20′W	94.9	LADCP+CTD
Semane2000.2	09/2000	S04	08°44′W	74.5	LADCP+CTD
		S05	08°32′W	74.0	
		S06	08°20′W	72.7	
Sflux	09/2011	S07	07°48′W	48.7	ADCP+CTD
		S08	07°25′W	32.1	
		S09	08°08′W	23.0	
		S10	07°25′W	19.6	

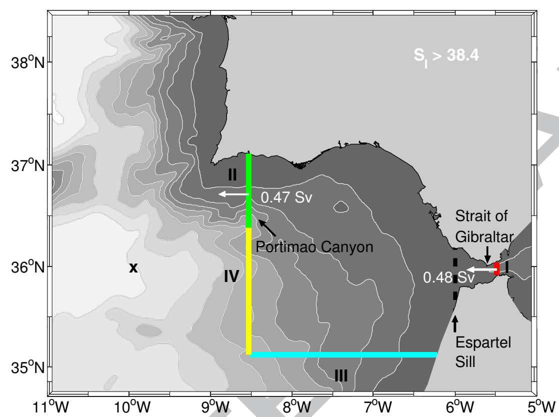

Figure 2: Domain of study with the main geographic references and topography in grey scale at regular intervals of 500 m. The dashed line represents the approximate location of Espartel Sill. The reference location is marked with an "x". In colour is represented the closed domain of the Lagrangian experiments: e.g. particles released at the Strait of Gibraltar (section I) are followed until crossing sections II, III and IV. The numbers correspond to the mean westward transport originating in section I and crossing II (average of transports over 10 yrs).

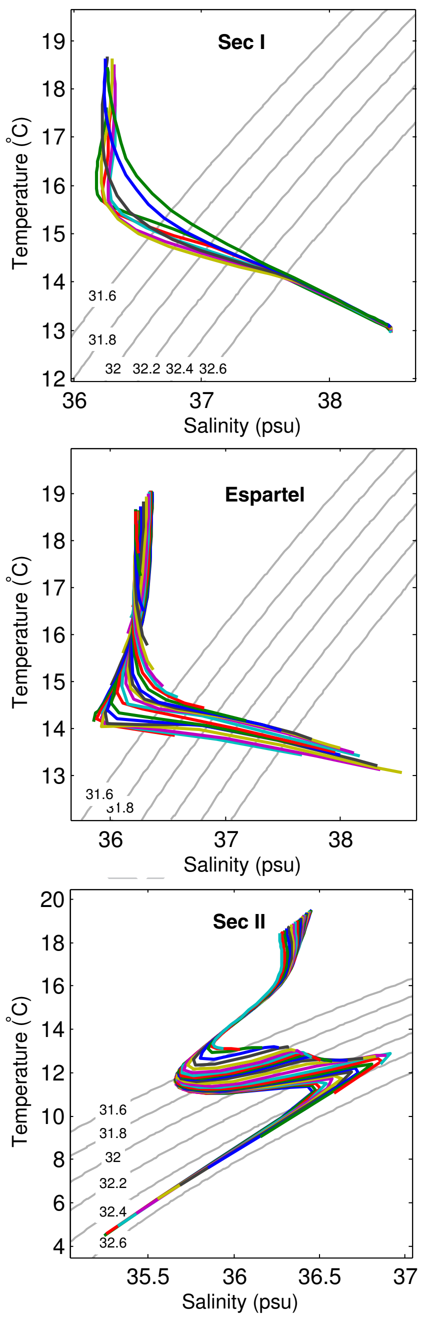

Figure 3: Model's output: time-averaged TS-diagrams from section I ($\lambda \sim 5°30'$W), near-Espartel section ($\lambda \sim 6°$W) and section II ($\lambda \sim 8°30'$W). Each coloured line corresponds to a different grid-point.

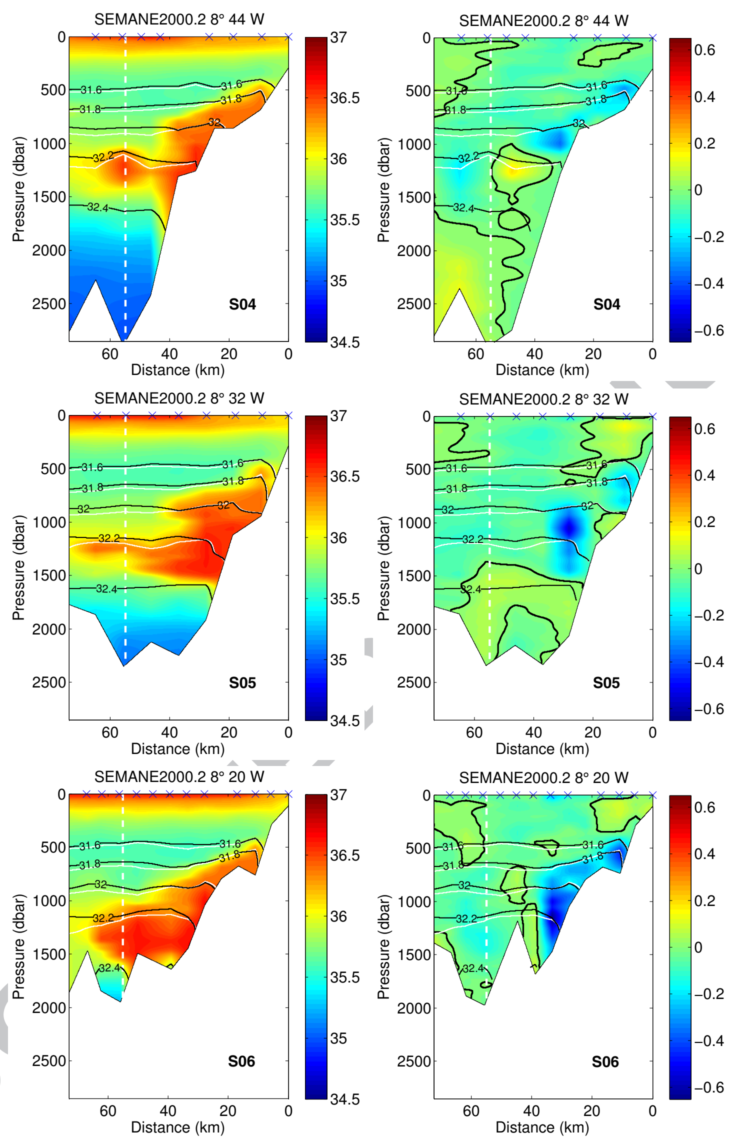

Figure 4: Salinity field (left, psu) and zonal velocity (right, m s^{-1}) from sections S04, S05 and S06 (west to east, respectively, see Figure 1). The dashed-vertical line highlights the 55 km limit imposed in the transport calculations. The crosses identify the CTD/LADCP stations. The black (white) contours correspond to σ_1 (σ_0) in kg m^{-3} and the distance increases southwards. The isopycnals are shown at a regular interval of 0.2 kg m^{-3} and the thick line represents the inflow/outflow interface, i.e. the isoline of zero zonal velocity.

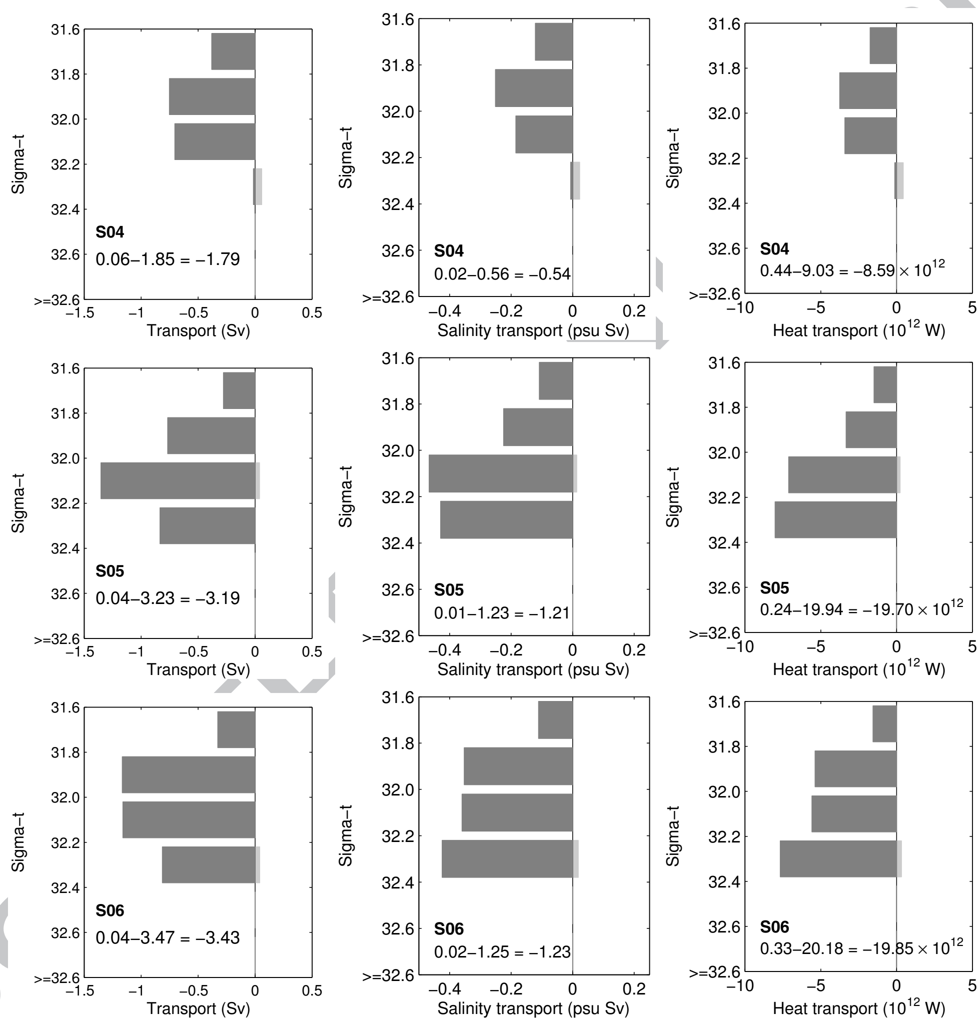

Figure 5: Volume, salinity and heat transports at sections S04, S05 and S06 from Semane. Printed in each graph are the totals (regarding the layers shown) $eastward - westward = net$. A mask was applied in order to retain only MW transport (section 4.2.1). 1 psu Sv = 1 kg salt/1000 kg seawater $\times 10^6$ m^{3}s^{-1} = 10^3 m^{3}s^{-1}.

Table 2: Westward volume transport in units of Sv (1 Sv= 10^6 m^3 s^{-1}) per density layer, from observational data. A mask was applied in order to retain only MW transport (section 4.2.1).

	31.6 − 31.8	31.8 − 32.0	32.0 − 32.2	32.2 − 32.4	32.4 − 32.6	Total
S08 (7°25′W)	0.11	0.05	0	0	0	0.16
S10 (7°25′W)	0.15	0.1	0	0	0	0.24
S07 (7°48′W)	0.25	0.41	0.01	0	0	0.67
S09 (8°08′W)	0.34	0.56	0.07	0	0	0.97
S03 (8°20′W)	0.28	0.83	0.94	0.53	0.03	2.61
S02 (8°20′W)	0.40	0.87	1.20	1.13	0	3.60
S06 (8°20′W)	0.33	1.17	1.16	0.81	0	3.47
S05 (8°32′W)	0.28	0.77	1.35	0.83	0	3.23
S01 (8°32′W)	0.31	0.98	1.01	0.50	0	2.81
S04 (8°44′W)	0.38	0.75	0.70	0.01	0	1.85

Table 3: Pure MW mask computed from the properties of particles seeded in I and arriving at section II (section 4.2.1, Figure 9). Per density layer: mean salinity and temperature values plus or minus three times their standard deviation.

σ_1 (kg m^{-3})	T_{min} (°C)	T_{max} (°C)	S_{min} (psu)	S_{max} (psu)
31.6–31.8	11.27	14.14	35.70	36.59
31.8–32.0	10.96	13.83	35.86	36.65
32.0–32.2	11.21	13.28	36.13	36.86
32.2–32.4	11.08	13.47	36.38	37.10
32.4–32.6	8.64	14.10	36.02	37.30

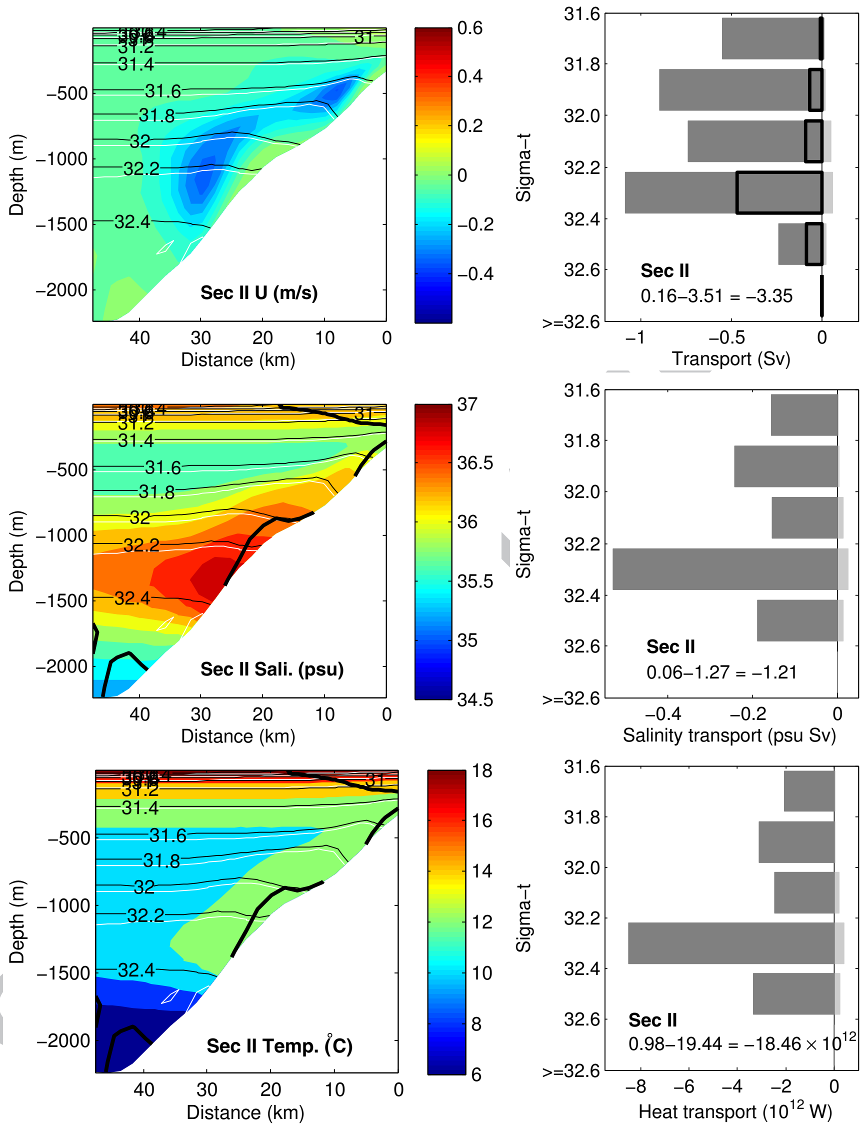

Figure 6: Model's output: 1989-1998 time-averaged results at section II, $\lambda \sim 8°30'$W. The totals (regarding the layers shown) $eastward - westward = net$ are printed in the graphs. A mask was applied in order to retain only MW transport (Table 3). The thick-black lines represent the transport originating in I (seeding in the whole water column) and arriving to II. The difference in size of the grey and black bars is due to entrainment of NACW as the outflow progresses along the northern boundary of the Gulf of Cadiz. Contour lines: same as in Figure 4.

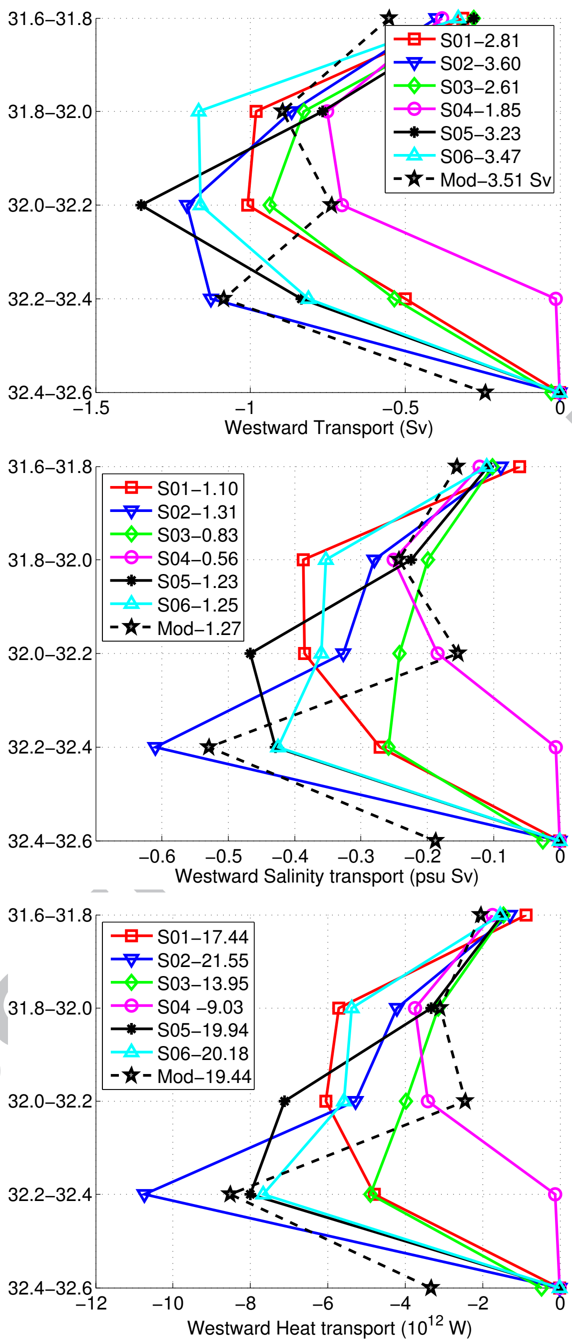

Figure 7: Westward MU transport of volume (top), salinity (middle) and heat (bottom) per density layer from Semane data (S01-S06) and the model's (Mod) shelf section (coincident with S05), using a mask to retain only MW transport (section 4.2.1). The totals (westward and within the layers shown) are noted in the legends.

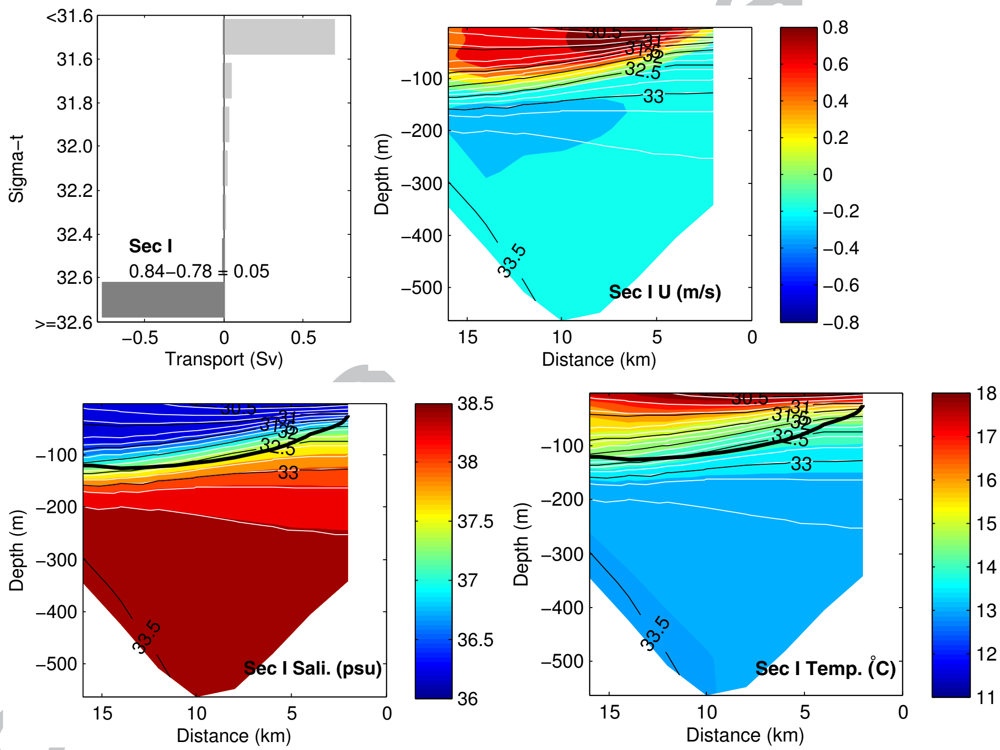

Figure 8: Model's output: 1989-1998 time-averaged volume transport, zonal velocity, salinity and temperature fields at section I. Contour lines: same as in Figure 4.

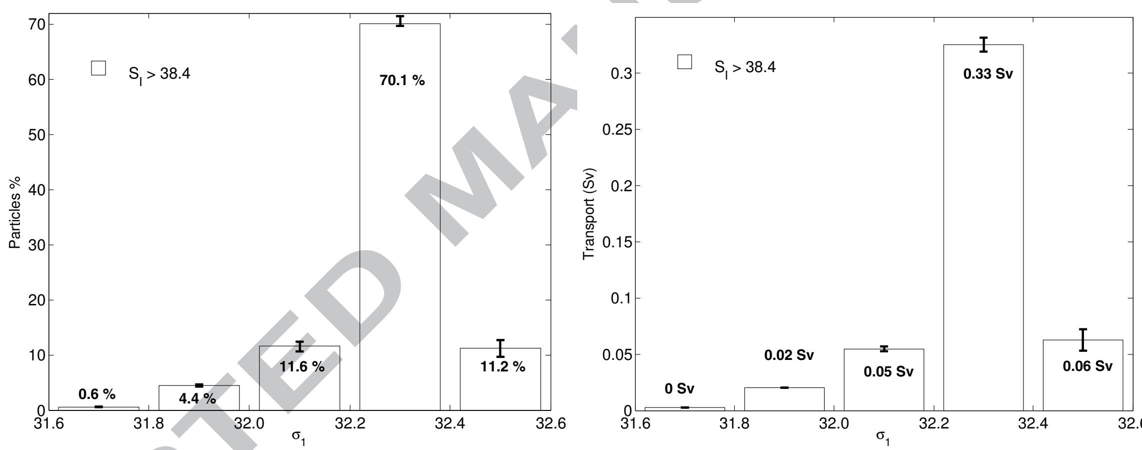

Figure 9: Time-averages for the period of 1989-1998, computed by releasing particles at section I in pure MW ($S > 38.4$ psu); the errorbars reflect the variation over the period. Percentage of particles (left) and Lagrangian transport (right) reaching section II, per density layer.

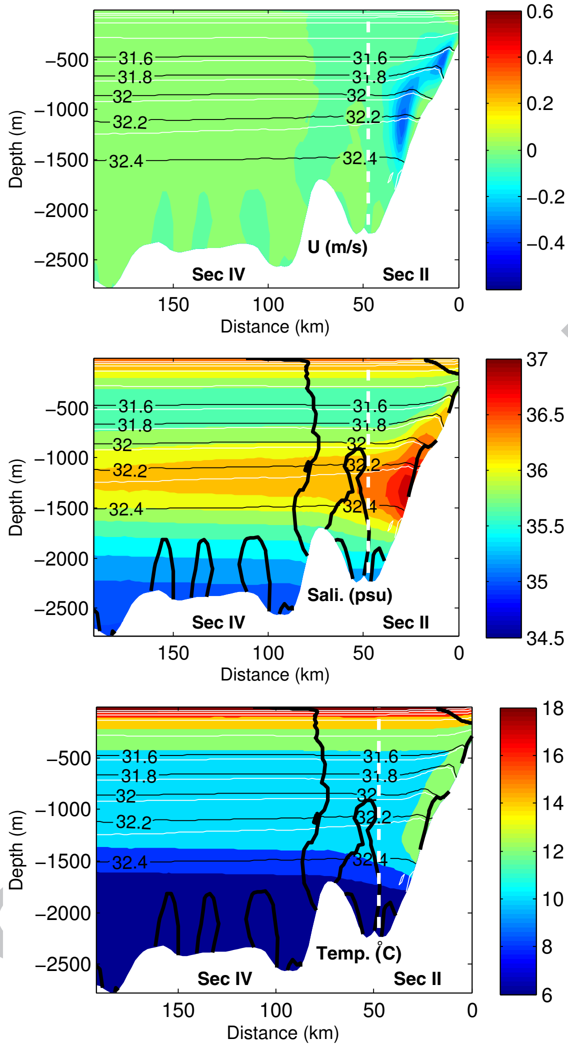

Figure 10: Model's output: 1989-1998 time-averaged zonal velocity, salinity and temperature fields at sections II and IV. The white-dashed line splits the two sections. Contour lines: same as in Figure 4.

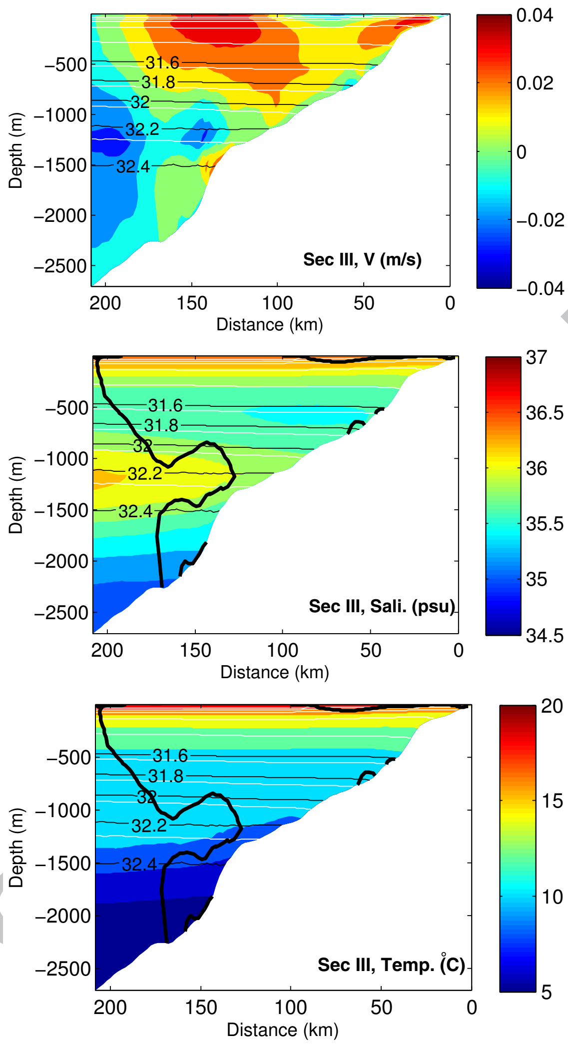

Figure 11: Model's output: 1989-1998 time-averaged meridional velocity, salinity and temperature fields at section III. Contour lines: same as in Figure 4.

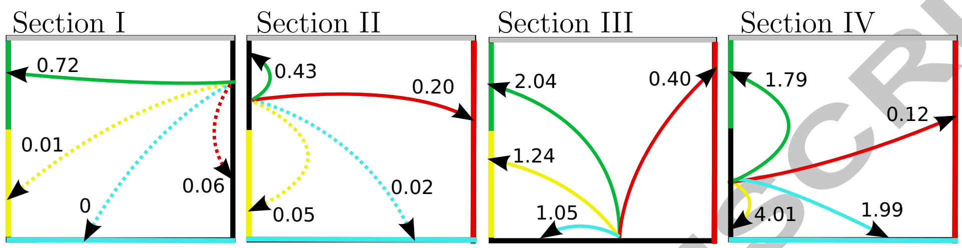

Figure 12: Summary of total time-averaged Lagrangian transports [Sv] originating/arriving in/to each section (whole water column) of the closed domain shown in Figure 2. The four charts illustrate the overall results of four experiments: seeding of particles in sections I, II, III and IV separately; in each case, the section of origin is in black whereas the section of arrival is colour-coded according to Figure 2. The grey line represents the northern slope/coast of the Gulf of Cadiz. The arrows in dotted lines indicate transports smaller than 0.1 Sv. In each chart, the sum of all arrows corresponds to the negative values in line 'Lagr-Total' of Table 4.

Table 4: Time-averaged Lagrangian volume transport [Sv] per density layer, for each section of the closed domain (see Figure 2). Positive (negative) values refer to transport out (into) of the domain. Balance: net transport per density layer; negative (positive) values stand for volume loss (gain). Total_I: transport out of the domain (sum of all sections) originating in section I. Lagr-Total: transport per section, sum of all layers. $\sigma_2 \geq 36.9$: refined calculations of transport in the deepest layer to assess entrainment due to NADW.

σ_1 (kg m^{-3})	I	II	III	IV	Balance	Total_I
< 31.6	0.66 - 0	1.08 - 0.39	0.64 - 2.31	1.17 - 1.91	-1.07	0.01
31.6–31.8	0.05 - 0	0.73 - 0.03	0.21 - 0.65	0.45 - 0.78	-0.02	0.01
31.8–32.0	0.03 - 0	0.96 - 0.03	0.27 - 0.48	0.48 - 0.82	0.40	0.08
32.0–32.2	0.02 - 0	0.81 - 0.06	0.44 - 0.37	0.64 - 1.03	0.45	0.11
32.2–32.4	0.01 - 0	1.05 - 0.08	0.67 - 0.39	1.09 - 1.46	0.89	0.49
32.4–32.6	0.01 - 0.01	0.35 - 0.10	0.83 - 0.53	1.48 - 1.91	0.13	0.09
≥ 32.6	0 - 0.77	0 - 0	0 - 0	0 - 0	-0.77	0
Lagr-Total	0.79-0.79	4.98 - 0.70	3.06 - 4.73	5.31 - 7.91	0	0.79
$\sigma_2 \geq 36.9$	-	0.09 - 0.07	0.58 - 0.35	0.97 - 1.31	-0.09	-

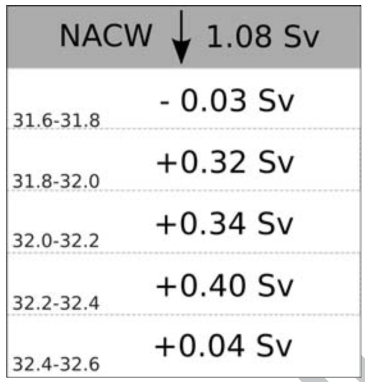

Figure 13: Sketch of entrainment of NACW within the closed domain in the Gulf of Cadiz. Computed by subtracting 'Total_I' to 'Balance', layerwise (see Table 4).

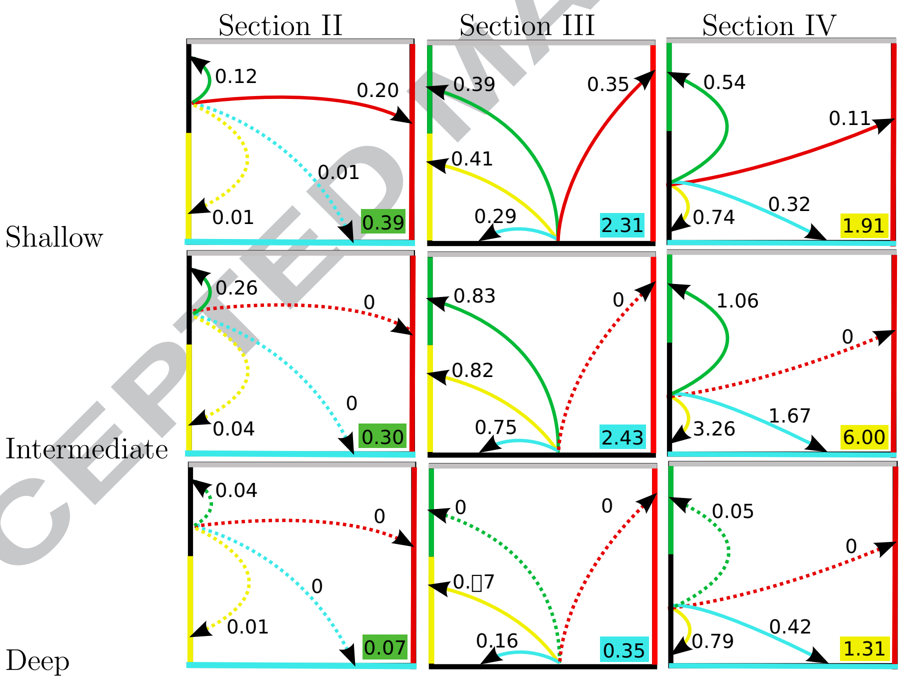

Figure 14: Time-averaged Lagrangian transports [Sv] originating/arriving in/to each section in the GoC per main layer: Shallow $\sigma_1 < 31.6$ kg m^{-3} (top), Intermediate $31.6 \leq \sigma_1 < 32.6$ kg m^{-3} (middle) and Deep $\sigma_2 \geq 36.9$ kg m^{-3} (bottom). Legend as in Figure 12; the transport into the domain (in the seeding section and layer) is indicated here in the lower right corner of each chart. Note the difference in total transport into and out of the domain in the Shallow layer, sections III and IV.

Appendix A. Volume, salinity and heat transports

The volume transport (T_V) was computed by considering all cells whose density value fell within the specified limits:

$$T_V(\sigma_i) = \sum_k \sum_j u_{jk}\delta_j\delta_k \ , \quad j,k \in [\sigma_i, \sigma_{i+1}[\tag{A.1}$$

where j,k are the meridional and vertical indices of a grid cell with length δ_j and height δ_k. There will be a small error introduced by assuming that all cells are rectangular, but this should not be very significant since the assumption only fails for those cells in the immediate vicinity of the slope.

Salinity and heat transports (S_f and Q_f) were computed per density interval and with respect to a location out of reach of the Mediterranean outflow at 10°W-36°N, as follows

$$\begin{aligned} S_f(\sigma_i) &= \sum_k \sum_j (S_{jk} - S_0^i) u_{jk}\delta_j\delta_k \ , \quad j,k \in [\sigma_i, \sigma_{i+1}[\\ Q_f(\sigma_i) &= \sum_k \sum_j c_p(\sigma_{jk} + 1000)(T_{jk} - T_0^i) u_{jk}\delta_j\delta_k \end{aligned}$$

where S_0^i (T_0^i) is the mean salinity (temperature) at the reference location and corresponding density interval i, and $c_p = 4 \times 10^3$ J kg^{-1} °C^{-1} (Chambers et al., 1997; Warren, 1999). The salinity and temperature profiles used as reference for observational and numerical results were distinct. In the first case, these were taken from a climatological dataset (Locarnini et al., 2006; Antonov et al., 2006) whereas in the latter they correspond to the numerical output time-averaged profiles at the reference location (see Figure 2); no reference was used for depths greater than 2000 m since the influence of the MW beyond such level is assumed to be negligible. The model results presented correspond to an Eulerian mean: the transport was first computed at each instant of time and then time-averaged.